Contact Resistance in Monolayer MoS_2 Edge-Contacts: "Electrostatic" *vs*. Substitutional Doping

Madhuchhanda Brahma
Dept. of Materials Science & Engineering
The University of Texas at Dallas
Richardson, USA
madhuchhanda.brahma@utdallas.edu

Maarten L. Van de Put
Dept. of Materials Science & Engineering
The University of Texas at Dallas
Richardson, USA
maarten.vandeput@utdallas.edu

Edward Chen
Corporate Research
Taiwan Semiconductor Manufacturing Company Ltd.,
Hsinchu, Taiwan
chenjhm@tsmc.com

Massimo V. Fischetti
Dept. of Materials Science & Engineering
The University of Texas at Dallas
Richardson, USA
max.fischetti@utdallas.edu

William G. Vandenberghe
Dept. of Materials Science & Engineering
The University of Texas at Dallas
Richardson, USA
william.vandenberghe@utdallas.edu

2024 International Conference on Simulation of Semiconductor Processes and Devices (SISPAD) | 979-8-3315-1635-2/24/$31.00 ©2024 IEEE | DOI: 10.1109/SISPAD62626.2024.10733092

***Abstract*— We present results on the effect of a surrounding dielectric and a back-gate bias on the resistance of "electrostatically" doped two-dimensional (2D) materials edge-contacts and compare it to contacts to impurity-doped 2D materials. The transmission probability is computed using the Wentzel–Kramers–Brillouin approximation, the full-band density of states obtained from density functional theory, and the potential is obtained from the 2D Poisson's equation. We find that a low-κ back-gate oxide with a low-κ top dielectric environment results in a lower contact resistance in "electrostatically" doped edge-contacts. The image-force barrier-lowering is reduced by the back-gate, whereas in impurity doped contacts, it is determined by the dielectric permittivity of the surrounding oxide and of the 2D material. Additionally, we observed that in all cases, "electrostatically" doped devices exhibit worse contact resistance than impurity doped ones, and only very high gate bias, such as > 1V, can yield sufficiently low contact resistance when using a high- κ back gate oxide.**

Keywords—metal/TMD, edge-contact, WKB, 2D Poisson, image force, dielectric, back-gate

I. Introduction

Two-dimensional (2D) materials, particularly transition metal dichalcogenides (TMDs), show promise for future electronic devices due to their unique electronic properties. However, challenges, such as high Schottky barrier [1, 2] and Fermi level pinning [1, 2], result in a high contact resistance and limit their practical application. Quantum-transport models based on density functional theory (DFT) [3, 4] offer insights but face computational limits and cannot account for the effect of image-force barrier lowering (IFBL), which is always present in any metal-semiconductor contact. Indeed, our prior work demonstrates that the surrounding dielectrics significantly influence the contact resistance by modulating the depletion length and the Schottky-barrier lowering [5]. We found that low-κ dielectrics are beneficial for reducing contact resistance, unlike high-κ dielectrics, which worsen it due to an increased depletion width and a reduced IFBL [5].

Various doping methods, like substitutional, charge-transfer, and electrostatic doping, are explored to minimize the contact resistance [6-9]. Substitutional doping can introduce defects, while charge-transfer doping uses adsorbed dopants to achieve n-type or p-type behavior. On the other hand, "electrostatic doping", achieved through gate voltage manipulation, is non-destructive and reversible.

In this paper we assess the contact resistance of 2D material edge-contacts quantitatively, assuming "electrostatic" doping (*i.e.* doping the channel by changing the back-gate voltage), and emphasize the need for low-κ dielectrics, and highlight the limitations of doping by back-gate compared to the conventional impurity-doping. We calculate numerically the contact resistance using the full-band density of states obtained from DFT calculations of MoS_2 and use the WKB approximation to calculate the transmission probability through the Schottky barrier at the metal-MoS_2 interface.

In the first section of the paper, "Methods", we describe the numerical and mathematical approach we used to calculate the contact resistance starting from DFT calculations. Next, in the "Results" section, we discuss the effect of the back-gate on the contact resistance and compare "electrostatically' doped contacts with impurity doped ones. Lastly, we conclude our findings in the "Conclusion" section.

II. Method

We consider an edge-contact geometry consisting of an undoped TMD monolayer (MoS_2) "sandwiched" between an infinitely thick top oxide (SiO_2 or HfO_2) and a thin bottom oxide with a metal back-gate (see Fig. 1 (a)). Assuming an ideal Schottky barrier, we exclude effects from interface chemistry, Fermi-level pinning, and band offsets. For impurity-doped contacts (without gate bias), we consider infinitely thick top and bottom oxides, while for "electrostatically" doped edge-contacts, we select a bottom oxide of finite thickness. Various device configurations, labeled A through F, were simulated, with

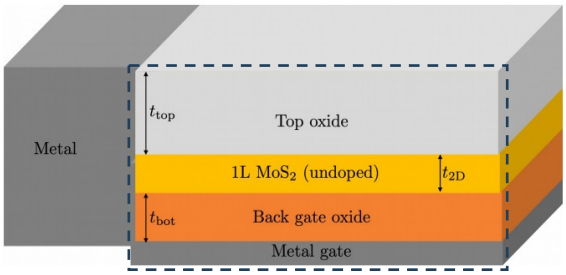

(a)

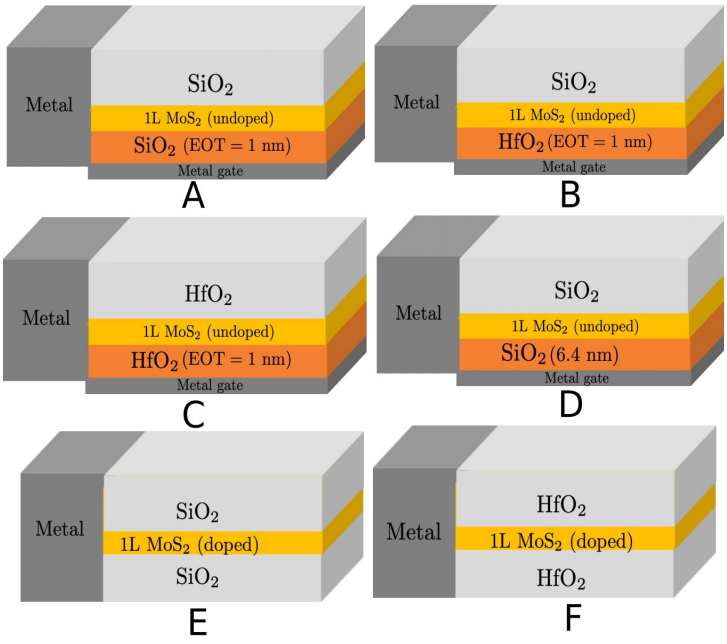

(b)

Fig. 1 (a). Edge-contact geometry considered here. The Poisson equation is solved over the 2D cross-section marked as a box. $t_{top} >> t_{2D}$ (b) The different edge-contact geometries considered in the simulation: A, B, and C denote the back-gated edge-contacts (back-gate oxides EOT=1 nm). D has a similar composition as A, but the back-gate oxide has a physical thickness of a HFO_2 with EOT of 1 nm. In A, B, C and D the top dielectric (either SiO_2 or HfO_2) is considered infinitely thick, and the back-gate oxide is either SiO_2 or HfO_2. E and F with infinitely thick top and bottom oxides, represent the geometries considered in our previous work [5], where the effect of gate-metal was not included.

configurations A, B, C, and D having back-gate ("electrostatically" doped) and E, F representing geometries from our previous work [5] *i.e.* with an impurity doped TMD, as shown in Fig. 1 (b).

In our previous work [5], we compared contact resistances calculated using the WKB approximation and the NEGF formalism, finding close agreement with a slight overestimation of the conductance when using the WKB approximation [5]. Due to large simulation domain requirements and the inability to treat image-force barrier lowering using DFT-NEGF simulations, we use the WKB approximation to determine the transmission probability through the Schottky barrier at the metal-TMD junction. Contact resistance is numerically calculated using Eq. 1 [10]:

$$\frac{1}{\rho_C} = \int_{-\infty}^{\infty} \frac{2e^2}{h} \left\{ \int \left[\sum_n M_n(k_y, E)\, T_n(k_y, E) \right] \frac{dk_y}{2\pi} \right\} \left| \frac{\partial f(E)}{\partial E} \right| dE \quad (1)$$

where e is electronic charge, h is Planck's constant, $f(E)$ is the Fermi-Dirac distribution at energy E. The band dispersion $E_n(k_x, k_y)$, is obtained from the DFT calculations (performed using the software package VASP [11]), and n is the band index.

The electrostatic potential required to calculate the WKB tunneling probability $T_n(k_y, E)$ is obtained by solving the Poisson equation using finite elements [12-13], over the 2D cross-section show in Fig. 1(a), with Dirichlet boundary conditions at the metal contact and back gate, and an anisotropic dielectric permittivity for MoS_2 (in-plane and out-of-plane permittivity being $15.5\epsilon_0$ and $6.2\epsilon_0$, respectively [14]).

We calculate the band structure of monolayer MoS_2 using VASP [10], employing the GGA [15] with the PAW method [16-18] for geometry optimization and the HSE06 hybrid functional [19] with spin-orbit coupling for electronic calculations. The band structure is interpolated on a denser k-mesh using maximally localized Wannier functions in the Wannier90 code [20] to compute the transmission probability.

To account for the image force barrier lowering, we first calculate the Coulomb kernel of a point charge in the cross-section shown in Fig. 1(a), which is as follows:

$$\hat{V}_{image}(Q, z=0) = -\frac{\left[\epsilon_{2D}\cosh(aQ) + \epsilon_{top}\sinh(aQ)\right]\left[\epsilon_{2D}\cosh(aQ)\sinh(t_{bot}Q) + \epsilon_{bot}\sinh(aQ)\cosh(t_{bot}Q)\right]}{\epsilon_{2D}Q\left[\epsilon_{top}\epsilon_{bot}\cosh(t_{bot}Q) + \epsilon_{2D}^2\sinh(t_{bot}Q) + \epsilon_{2D}\cosh(2aQ)\left\{\epsilon_{bot}\cosh(t_{bot}Q) + \epsilon_{top}\sinh(t_{bot}Q)\right\}\right]} \quad (2)$$

where ϵ_{2D}, ϵ_{top}, and ϵ_{bot} represent the dielectric permittivity of the 2D material ($\epsilon_{2D} = \sqrt{\epsilon_\perp \epsilon_\parallel}$, where $\epsilon_\parallel$ and $\epsilon_\perp$ are the in-plane and out-of-plane dielectric permittivity of monolayer MoS_2) and of the top and bottom oxides, respectively, whereas a, t_{top}, and t_{bot} denote one-half of the 2D material thickness and the top and bottom oxides respectively. Finally, we calculate the image numerically [5] by applying the two dimensional Fourier Bessel transform and the method of images [5] on Eq. 2.

III. RESULTS AND DISCUSSION

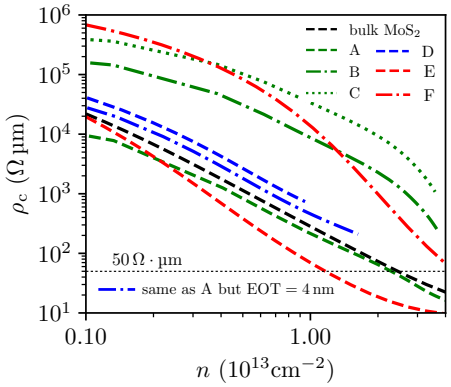

Fig. 2. Calculated contact resistance vs. doping concentration for MoS_2 edge-contacts with a Schottky barrier height of 0.3 eV. The lowest contact resistance is obtained with top and bottom insulators as SiO_2 in configurations with both back-gate and without back-gate. i.e. A and E. The blue lines do not span the entire density range because we limit back-gate bias to 4 V. Since a back-gate oxide as SiO_2 with EOT of 1nm is subjected to considerable gate leakage, we also simulate a device with a similar configuration as A but with EOT of 4nm.

Figure 2 shows the relationship between contact resistance and doping concentration, comparing bulk and edge-contact configurations, with and without a back-gate. The lowest contact resistance is found in impurity-doped edge-contacts surrounded by a low-κ dielectric (geometry E). Among the back-gated devices, device A, with SiO_2 as the top and bottom oxides, shows the lowest contact resistance, slightly outperforming the bulk configuration. A doping concentration of 2×10^{13} cm^{-2} results in a contact resistance as low as 50 Ω·µm in edge-contact configuration A, while higher concentrations are needed for other "electrostatically" doped configurations.

Figure 3 indicates that the contact resistance in configuration A increases by up to 2.5 times compared to its no-gate counterpart E. A similar trend is seen in configuration C, with an 11-fold increase in contact resistance *w.r.t.* F, highlighting the disadvantage of doping by back-gate. In geometry B, the contact resistance increases 2.5-fold relative to F and 100-fold relative to E. Among the "electrostatically" doped contacts with the same EOT, configuration A (low-κ back-gate oxide) performs better than B. Between B and C (both high-κ back-gate oxide but different top dielectric environment), configuration C (HfO_2 top oxide) shows a worse contact resistance. These results highlight the importance of the dielectric environment and back-gating for the optimization of contacts to 2D materials.

The choice of back-gate oxide influences the contact resistance through the depletion width and the image-force barrier lowering (IFBL). At a given EOT, the largest depletion width occurs when high-κ dielectrics are used as both the back-gate oxide and the thick top-dielectric environment. The use of high-κ materials as top- or back-gate oxides increases electric field screening. At a given EOT, high-κ back-gate oxides, such as HfO_2, are physically thicker and results in a larger depletion width compared to SiO_2 due to enhanced fringing field-screening. Fig. 4 demonstrates that at a given back-gate bias, the potential energy drops sharply with SiO_2 as the back-gate oxide, leading to a shorter depletion tail inside the channel, and hence the thinnest depletion width. Configuration B, with a low-κ back-gate oxide and a high-κ top oxide, has a slightly larger depletion width. Configuration C, with high-κ oxides for both top and back-gate dielectrics, shows the largest depletion width. A smaller depletion width reduces tunneling distance, increasing transmission probability and reducing contact resistance, as observed in geometry A.

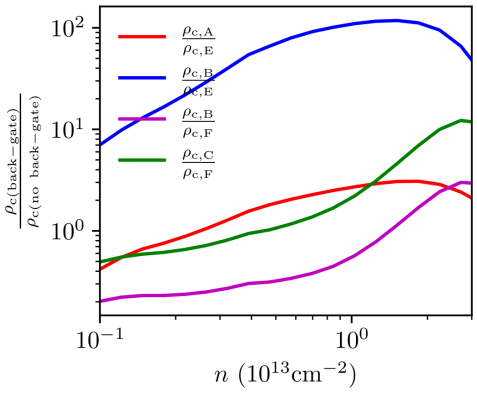

Fig. 3. Ratio of contact resistances of configurations A, B, and C as a function of doping concentration, to their non-gate counterparts E and F.

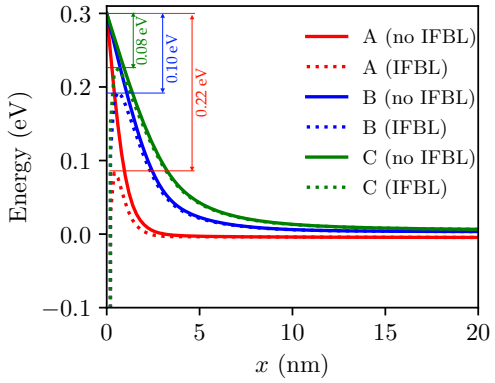

Fig. 4. Potential energy in back-gate devices A, B and C plotted with and without taking into effect IFBL. The 1D cuts are obtained from the 2D potential profiles we get by solving the Poisson equation.

From Fig. 4 we also find that at a fixed gate bias (1V shown) the barrier lowering is the smallest in configuration C and highest in configuration A. The proximity of the gate-metal further aids in reducing the barrier height, with low-κ insulators lowering the barrier more effectively than high-κ oxides at a given EOT. Figure 5 shows the inverse of the image potential energy with respect to the distance from the metal-TMD interface. For distances much larger than the layer thickness, the inverse image potential is determined by the back-gate, contrasting with the case without a back-gate (*i.e.* impurity doped contact) where it is determined by the surrounding oxide's dielectric constant. Close to the interface, the 2D material's dielectric constant dominates, like the bulk case. This indicates that the back-gate screens the barrier lowering effect, hindering the improvement in contact resistance in electrostatically doped edge-contacts.

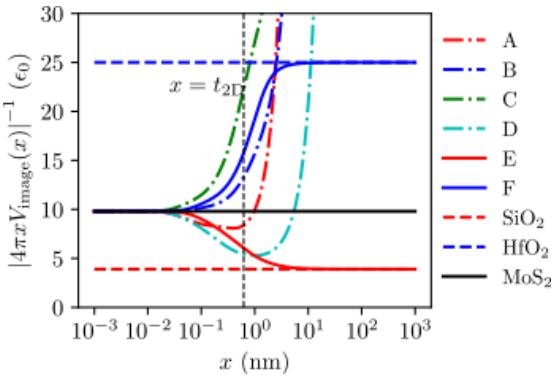

Fig. 5. Reciprocal of image potential energy plotted as a function of the distance from the metal-TMD interface. Low values of $(4\pi x V_{\text{image (x)}})^{-1}$ means improved IFBL and therefore E and A have the best cases of barrier lowering.

IV. Conclusion

We have evaluated numerically the contact resistance of back-gated ("electrostatically' doped) metal-TMD edge-contacts, considering both low-κ and high-κ bottom oxides with similar EOTs. Low-κ back-gate oxides result in a lower contact resistance, though gate leakage is a concern due to thinner gate-oxides. A high gate bias (>1V) can result in a favorable contact resistance (50 Ω µm) with high-κ back-gate oxides like HfO_2. We accounted for semiconductor doping via back-gate bias in our simulations and found that "electrostatically" doped edge-contacts do not offer significant benefits compared to impurity-doped ones.

Acknowledgment

This work has been supported by Taiwan Semiconductor Manufacturing Company, Ltd and NEWLIMITS/nCORE program of the Semiconductor Research Corporation (SRC). We also acknowledge the Texas Advanced Computing Center (TACC) at The University of Texas at Austin for providing the high-performance computing resources.

References

[1] S. Das, and J. Appenzeller, "Where does the current flow in two-dimensional layered systems?" Nano Letters, vol. 13, pp. 3396-402, Jul 2013.

[2] A. Allain, J. Kang, K. Banerjee, and A. Kis, "Electrical contacts to two-dimensional semiconductors," Nature Materials, vol. 14, pp. 1195-1205, Dec. 2015.

[3] K. Parto, A. Pal, T. Chavan, K. Agashiwala, C.-H. Yeh, W. Cao, and K. Banerjee, "One-Dimensional Edge Contacts to Two-Dimensional Transition-Metal Dichalcogenides: Uncovering the Role of Schottky-Barrier Anisotropy in Charge Transport across MoS_2/Metal Interfaces", Physical Review Applied, vol. 15, pp. 064068, June 2021.

[4] A. Szabo, A. Jain, M. Parzefall, L. Novotny, and M. Luisier, "Electron transport through metal/MoS_2 interfaces: edge-or area-dependent process?", Nano Letters, vol. 19, pp. 3641–3647, May 2019.

[5] M. Brahma, M. L. Van de Put, E. Chen, M. V. Fischetti, and W. G. Vandenberghe, "The importance of the image forces and dielectric environment in modeling contacts to two-dimensional materials", npj 2D Materials and Applications, vol. 7, March 2023.

[6] C. Huang, S. Wu, A. M. Sanchez, J. J. Peters, R. Beanland, J. S. Ross, P. Rivera, W. Yao, D. H. Cobden, and X. Xu, "Lateral heterojunctions within monolayer $MoSe_2$–WSe_2 semiconductors", Nature Materials, vol. 13, pp. 1096-1101, Aug 2014.

[7] V. P. Pham and G. Y. Yeom, "Recent advances in doping of molybdenum disulfide: industrial applications and future prospects", Advanced Materials, vol. 28, pp. 9024-9059, Aug 2016.

[8] Y. Li, C.-Y. Xu, P. Hu, and L. Zhen, "Carrier control of MoS2 nanoflakes by functional self-assembled monolayers", ACS Nano, vol. 7, pp. 7795-7804, Aug 2013.

[9] M. A. Khan, M. F. Khan, S. Rehman, H. Patil, G. Dastgeer, B. M. Ko, and J. Eom, "Two-dimensional materials memory devices with floating metal gate for neuromorphic applications", Scientific Reports, vol. 20, p. 100438, Dec 2023.

[10] S. Ravandi, B. Fu, W. G. Vandenberghe, S. J. Aboud, and M. V. Fischetti, "Pseudopotential-based study of gate leakage and contact resistance beyond the 10 nm node", 16th International Workshop on Computational Electronics, Jun 2013.

[11] G. Kresse and J. Furthmüller, "Software VASP, vienna, 1999", Physical Review B, vol. 54, pp. 169, 1996.

[12] M. S. Alnæs, J. Blechta, J.N Hake, A. Johansson, B. Kehlet, A. Logg, C. Richardson, J. Ring, M. E. Rognes, and G. N. Wells., "The fenics project version 1.5." Archive of Numerical Software, vol. 3, pp. 9-23, Dec 2015.

[13] A. Logg, K. A. Mardal, G. N. Wells, *et al*. "Automated Solution of Differential Equations by the Finite Element Method', Springer, 2012.

[14] A. Laturia, M. L. Van de Put, and W. G. Vandenberghe., "Dielectric properties of hexagonal boron nitride and transition metal dichalcogenides: from monolayer to bulk," npj 2D Materials and Applications, vol. 2, pp. 1–7, Mar 2018.

[15] J. P. Perdew, K. Burke, and M. Ernzerhof, "Generalized gradient approximation made simple," Physical Review Letters, vol. 77, p. 3865, Oct 1996.

[16] G. Kresse, and J. Furthmuller, "Efficient iterative schemes for *ab initio* total- energy calculations using a plane-wave basis set," Physical Review B, vol. 54, p. 11169, Oct 1996.

[17] G. Kresse, and J. Furthmuller, "Efficiency of *ab-initio* total energy calculations for metals and semiconductors using a plane-wave basis set," Computational Materials Science, vol. 6, pp.15–50, Jul 1996.

[18] G. Kresse, and D, Joubert, "From ultrasoft pseudopotentials to the projector augmented-wave method," Physical Review B, vol. 59, p. 1758, Jan 1999.

[19] J. Heyd, G. E. Scuseria, and M. Ernzerhof, "Hybrid functionals based on a screened coulomb potential" The Journal of Chemical Physics, vol. 118, pp. 8207– 8215, May 2003.

[20] A. A. Mostofi, J. R. Yates, G. Pizzi, Y.S. Lee, I. Souza, D. Vanderbilt, and N.Marzari, "An updated version of wannier90: A tool for obtaining maximally-localised Wannier functions", Computer Physics Communications, vol. 185, pp.2309-2310, Aug 2014.